ACS EARTH AND SPACE CHEMISTRY

Article

Cite This: ACS Earth Space Chem. 2018, 2, 235−245

Effect of Photolysis on Absorption and Fluorescence Spectra of Light-Absorbing Secondary Organic Aerosols

Paige K. Aiona,[†] Jenna L. Luek,[‡] Stephen A. Timko,[‡] Leanne C. Powers,[‡] Michael Gonsior,[‡] and Sergey A. Nizkorodov*[,†]

[†]Department of Chemistry, University of California, Irvine, California 92617, United States

[‡]Chesapeake Biological Laboratory, University of Maryland Center for Environmental Science, Solomons, Maryland 20688, United States

Supporting Information

ABSTRACT: Excitation−emission matrices (EEMs) constructed from fluorescence measurements are increasingly used for the characterization of chromophoric dissolved organic matter (CDOM) and light-absorbing atmospheric organic aerosols known as brown carbon (BrC). There is a high uncertainty in the effect of BrC aerosols on climate because their optical properties depend on the amount of time they spent in the atmosphere. In order to aid in the quantification of BrC aerosols' contribution to radiative forcing, we investigated the effect of solar radiation on the fluorescence, expressed as EEMs, and absorption spectra of the water-soluble fraction of BrC species formed by the high-NOx photooxidation of benzene, toluene, *p*-xylene, and naphthalene. The BrC samples were prepared in a smog chamber, extracted in water, and irradiated in a solar simulator at a fixed pH of 3, representative of aerosol liquid water, or at a fixed pH of 6, representative of cloudwater. Semicontinuous fluorescence and absorbance measurements were carried out during the irradiation at 20 min intervals for 44 h. The absorption coefficients depended on the solution pH, with the solutions at pH 6 absorbing stronger than solutions at pH 3. All samples underwent a decrease in absorption coefficient at all visible wavelengths, whereas fluorescence intensities showed both increases and decreases in different regions of the EEMs. Upon comparison with CDOM samples, the fluorescence intensity of all secondary organic aerosol (SOA) samples decreased in the region of the EEMs where the characteristic terrestrial humic-like C peak occurs. These experimental observations suggest that (i) this type of BrC will have different effects on climate depending on whether it ends up in an acidic or neutral environment; (ii) exposure to UV radiation will diminish the ability of this type of BrC to affect climate on a time scale of about a day; (iii) fluorescence by BrC compounds has a minimal effect on aerosol radiative forcing; (iv) photooxidized aromatics may be closely related, in terms of optical properties, to CDOM found in fresh waters.

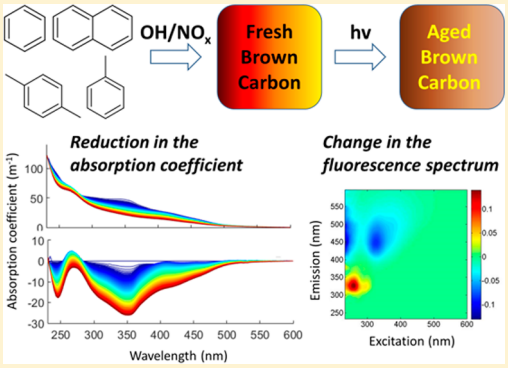

KEYWORDS: *Brown carbon, benzene, toluene, xylene, naphthalene, absorption coefficients, excitation emission matrix, apparent quantum yield*

INTRODUCTION

Fluorescence spectroscopy is commonly used to characterize different types of chromophoric dissolved organic matter (CDOM) in water samples from different systems.[1−3] Low levels of CDOM and small variation in its composition can be measured using fluorescence spectroscopy and excitation−emission matrices (EEMs) because these methods are much more sensitive than absorption spectroscopy.[4,5] Specific peaks in EEM spectra correspond to different chemical compositions of CDOM. Table 1 adapted from Coble lists the location of particular humic-, protein-, and pigment-like peaks due to fluorophores that are commonly found in natural water samples.[4,5] However, it should be noted here that other fluorophores have been suggested to give similar fluorescence than those described in Table 1.[6]

These peaks are subject to change due to environmental stress from mixing, biological degradation and production, and photochemical processes.[5] CDOM exposed to solar radiation is known to undergo photobleaching, which is accompanied by changes in its fluorescent properties.[1,2,7] Irradiation leads to a decrease in the fluorescence of the photolabile species in CDOM, but some materials such as tyrosine, tryptophan, and low molecular weight aromatic compounds may actually produce CDOM when exposed to irradiation.[2]

In contrast to the large number of fluorescence measurements for CDOM found in a variety of water systems,

Received: December 19, 2017
Revised: January 16, 2018
Accepted: January 22, 2018
Published: January 22, 2018

DOI: 10.1021/acsearthspacechem.7b00153
ACS Earth Space Chem. 2018, 2, 235−245

Table 1. List of Commonly Observed Peaks in EEMs Spectra of CDOM Found in Natural Water Systems as Described in Coble (1996 and 2007)

component	peak name	Ex_{max} (nm)	Em_{max} (nm)
tyrosine-like, protein-like	B	275	305−310
tryptophan-like, protein-like	T	275	340
UVC terrestrial humic-like	A	260	380−460
UVA terrestrial humic-like	C	320−360	420−480
UVA terrestrial humic-like		250 (385)	504
UVA marine humic-like	M	290−312	370−420
pigment-like	P	398	660

applications of fluorescence-based methods to describe organic compounds found in atmospheric aerosols remain limited.[8−14] Hawkins et al. compared fluorescence maps of aldehydes reacted with ammonium sulfate and glycine to those of water-soluble organic carbon extracts.[10] Matos et al. performed parallel factor analysis (PARAFAC) of EEMs collected for water-soluble and alkaline-soluble organic matter in extracts of urban aerosols.[9] Phillips and Smith used fluorescence measurements to explore the role of charge transfer complexes in absorption by organic compounds in particulate matter.[11,12] These fluorescence studies help distinguish different components of brown carbon (BrC) and allow for a more in depth understanding of its chemical and optical properties.

BrC is a subset of atmospheric particles containing molecules that strongly absorb visible and near-ultraviolet (UV) radiation. Upon deposition, BrC finds its way into ground waters and becomes part of CDOM. BrC can be produced by both primary sources, such as biomass burning, and by secondary reactions in the atmosphere.[15] Secondary organic aerosol (SOA) is formed by photooxidation of volatile organic compounds (VOCs), and for certain VOCs the oxidation products have a characteristic brown color. Examples include SOA produced by gas-phase photooxidation of naphthalene,[16] toluene,[17] xylene,[18] indole,[19] as well as by aqueous phase photooxidation of phenolic compounds[20,21] and other aromatic compounds.[22] In addition, reactive uptake of carbonyls and other organic compounds can also lead to BrC.[23−26] Some of these types of BrC are fluorescent and have been previously examined using EEMs.[9,15,27,28]

BrC SOA is a highly oxidized and complex system that may contain components that are similar to CDOM. These BrC species contain both water-soluble and insoluble components, with the water-soluble portion accounting for up to 70%.[15] Between 20 and 50% of water-soluble organic components in aerosols can be categorized as "humic-like substances" (HULIS).[29−32] The compositions of HULIS and CDOM found in natural water systems are similar with both containing heterogeneous mixtures of water-soluble, light-absorbing components.[29,33] Duarte et al. found the EEMs of water-soluble organic compounds in atmospheric aerosols produced fluorescence peaks similar to those of aquatic humic substances, with a shift to shorter wavelengths.[27]

Applications of fluorescence-based methods to BrC have provided valuable information about the effect of irradiation on its optical properties and composition. Lee et al. observed loss of absorption coefficient but gain in fluorescence from BrC produced from photooxidation of naphthalene.[16] Aiona et al. observed rapid removal of both chromophores and fluorophores from BrC produced by reaction between methyl glyoxal and ammonium sulfate.[34] Zhong and Jang reported a decrease in the fluorescence emission of extracts of wood smoke upon exposure to natural sunlight.[35] Within these studies the effect of photolysis on fluorescent characteristics of different types of BrC SOA has not been systematically investigated. None of the previous studies controlled the pH of the solution during irradiation, making it difficult to attribute changes solely to photolysis due to the high pH dependency of optical properties.[7]

In this study, EEM spectra, absorption spectra, and fluorescence quantum yields of BrC SOA are measured using a novel system that photolyzes aqueous extracts of BrC and simultaneously measures absorption and fluorescence spectra, while actively controlling the solution pH.[2,7] Benzene, toluene, *p*-xylene, and naphthalene are selected as representative secondary BrC precursors. We find that absorption coefficients for all BrC SOA decrease upon exposure to irradiation. In comparison, fluorescence decreases in certain regions of the EEMs, specifically in the area of the humic-like C peak, and increases in others. These changes in the humic region of the EEMs are characteristic of CDOM found in fresh water systems with terrestrial plant matter as the ultimate source.

1. EXPERIMENTAL SECTION

1.1. Formation of Secondary Organic Aerosols. SOA samples were generated in a ∼5 m^3 aerosol smog chamber via photooxidation under high-NO_x (NO_x refers to the sum of NO and NO_2) conditions for four different precursors: benzene, toluene, *p*-xylene, and naphthalene (abbreviated as BEN, TOL, XYL, and NAP, respectively). The chamber was flushed with clean air overnight and humidified to the desired level by filling it with air through a Nafion multichannel humidifier. Samples were prepared at 40% relative humidity (RH) in the chamber, except for a preliminary NAP SOA sample prepared under dry conditions (RH < 2%). The photochemical reactor (described below) required several milligrams of SOA material, so elevated concentrations of H_2O_2, NO_x, and each organic precursor had

Table 2. Summary of SOA Preparation Conditions[a]

precursor mixing ratio (ppm)	H_2O_2 (ppm)	NO_x (ppm)	RH (%)	photo-oxidation (h)	collection time (h)	mass collected (mg)	pH control	irradiation time (h)	C_{mass}[b] (mg/L)
NAP [0.4][c]	2.0	0.4	0	2	4	2	none	46	40
NAP [0.4]	2.0	0.4	40	2.3	4	1.8	3 and 6	44	36
TOL [1.5]	7.5	1.5	40	3.3	4	1.7	3 and 6	44	34
BEN [5.0]	15.0	0.5	40	3.7	4	1.7	3 and 6	44	34
XYL [2.0]	8.0	0.6	40	3.5	4	1.5	3 and 6	44	30

[a]Precursor abbreviations: "NAP", naphthalene; "TOL", toluene; "BEN", benzene; and "XYL", *p*-xylene; H_2O_2 and NO_x concentrations and relative humidity (RH) are listed before photooxidation. [b]Mass concentration of the SOA material in the solution assuming the SOA material could be fully extracted in 50 mL of water. [c]This sample was prepared under dry conditions to test the photolysis system without pH control.

DOI: 10.1021/acsearthspacechem.7b00153
ACS Earth Space Chem. 2018, 2, 235−245

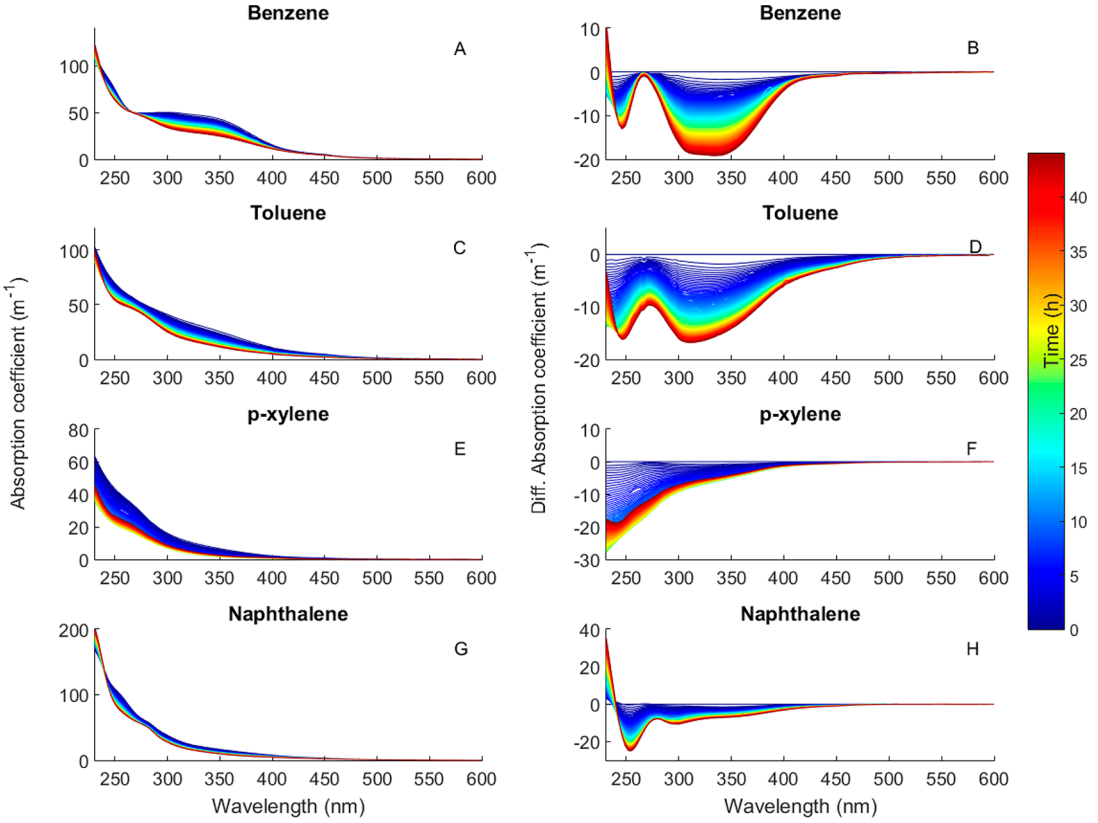

Figure 1. Comparison of solution absorption coefficients (m^{-1}, panels A, BEN SOA; C, TOL SOA; E, XYL SOA; and G, NAP SOA) and the change in absorption coefficient (panels B, BEN SOA; D, TOL SOA; F, XYL SOA; and H, NAP SOA) for each SOA over 44 h of irradiation at pH 3. If desired, these solution absorption coefficients can be converted into bulk MAC of the SOA material using eq 2.

to be used in order to obtain 1.5−2 mg of SOA sample (Table 2). H_2O_2 (Aldrich; 30% by volume in water) was evaporated into the chamber with zero air in mixing ratios ranging from 2 to 15 ppm to serve as a photochemical precursor to hydroxyl radicals. NO was added from a premixed cylinder to achieve initial NO_x concentrations ranging from 0.4 to 1.5 ppm. For NAP SOA samples, ∼23 μL of a 0.5 g/mL solution of naphthalene in dichloromethane was evaporated into the chamber to produce 0.4 ppm. Microliter volumes of pure toluene, benzene, or *p*-xylene were evaporated directly into the chamber to achieve initial mixing ratios of 7.5, 15.0, and 0.8 ppm, respectively. These concentrations are quite high by smog chamber standards, but they were necessary to produce sufficient amounts of material needed for the optical measurements described below. Chamber contents were mixed with a fan after addition before photooxidation, which was then initiated using UV−B lamps (Solar Tec Systems model FS40T12/UVB) with an emission centered at 310 nm. ThermoScientific monitors were used to monitor real time concentrations of NO/NO_y (model 42i-Y, NO_y refers to the sum of NO, NO_2, and other nitrogen containing compounds that can be catalytically reduced to NO) and ozone (model 49i), while temperature and RH were monitored with a Vaisala HMT330 probe enclosed in the chamber. Particle size distribution was monitored using a scanning mobility particle sizer (SMPS) (TSI Model 3936). The particle chemical composition was not tracked during the preparation. However, for NAP SOA prepared by Lee et al.[16] using a similar method, the average formula determined by high-resolution mass spectrometry was $C_{14.1}H_{14.5}O_{5.1}N_{0.085,}$ corresponding to an average O/C of 0.36.

Photooxidation lasted for 2−3.7 h (Table 2) and was stopped when the particle mass concentration in the chamber stopped growing. Particles were then collected for 4 h onto a PTFE filter at 15−20 standard liters per minute after passing through an activated carbon denuder. Collected SOA mass ranged from 1.5 to 2 mg, estimated from SMPS data assuming 100% collection efficiency by the filter (the actual mass was probably smaller since filters do not capture all the particles). Filters were then vacuum sealed and stored, before being sent to the University of Maryland for analysis. Because of the time-consuming nature of the measurements and data analysis, only one sample was prepared and examined for each of the SOA types.

1.2. Photolysis Experiments. A custom-built photolysis system was used to irradiate the SOA samples while simultaneously collecting absorbance and fluorescence data. SOA samples were extracted from filters using 50 mL of water and sonicated for 2 min, resulting in solution mass concentrations of the SOA compounds ranging from 30 to 40 mg/L (Table 1). We need to emphasize that this procedure only extracts water-soluble BrC components. However, the fraction of the water-insoluble compounds that remained on the filter is likely to be small because the brown-colored filter became white after the extraction. Indeed, NAP SOA prepared by a similar method by Lee et al. remained soluble to at least 0.6 g/L,[16] which is more than an order of magnitude higher than the concentrations used in this study. Samples were pumped through a spiral flow cell located underneath a solar

DOI: 10.1021/acsearthspacechem.7b00153
ACS Earth Space Chem. 2018, 2, 235−245

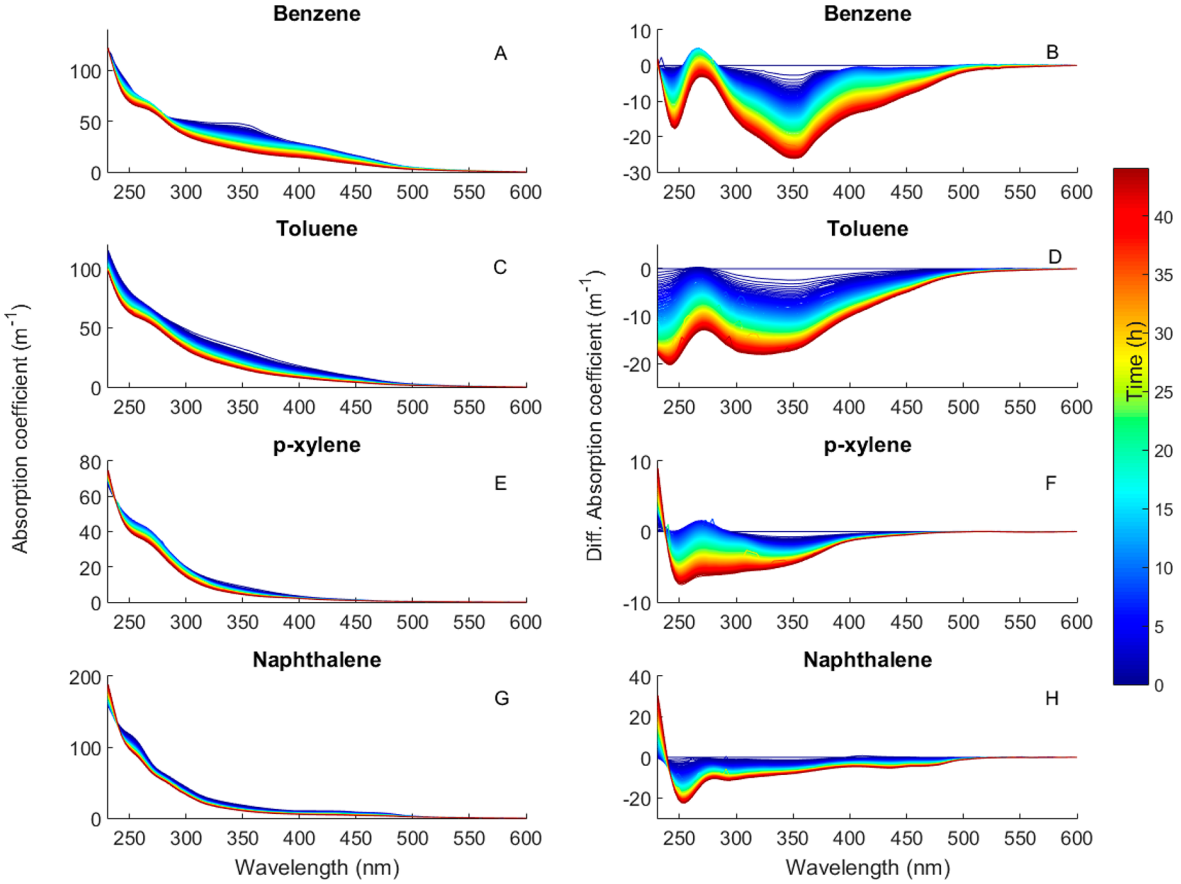

Figure 2. Comparison of solution absorption coefficients (m^{-1}, panels A, BEN SOA; C, TOL SOA; E, XYL SOA; and G, NAP SOA) and the change in absorption coefficient (panels B, BEN SOA; D, TOL SOA; F, XYL SOA; and H, NAP SOA) for each SOA over 44 h of irradiation at pH 6.

simulator using an inert micro gear pump. An Oriel Sol2A Class ABA solar simulator (Newport Corporation, Irvine, CA) with a 1000 W Xe arc lamp equipped with an AM 1.5 filter was used for irradiations. The solar spectrum of the lamp was set up to simulate the sun at a 48.2° solar zenith angle and an intensity of one sun (1 "sun" = 1000 W/m^2). Lamp power was controlled with a Newport 68951 Digital Exposure controller and its power was measured before each experiment with a Newport 91150 V Reference Cell. The spiral flow cell was custom built using SCHOTT Borofloat borosilicate glass (Hellma Analytics, 70 to 85% transmission between 300 and 350 nm, and 85% transmission at wavelengths >350) with a 2 mm wide by 1 mm deep flow path (total surface area of 101 cm^2).[7] The irradiation cell was temperature controlled to 25 °C using Peltier units and a recirculating water bath. Upon irradiating the photo reactor flow cell, the solution was injected into a 10 mL round-bottom flask with three necks, where the pH of the solution was monitored with a Thermo Orion 8220BNWP microelectrode. The pH was automatically adjusted as needed with a J-Kem Infinity II reaction controller coupled with a dual syringe pump using 0.1 M HCl or NaOH solutions. After passing through the air equilibrator, the sample was then drawn into the 4 × 10 mm flow cell of a Horiba Aqualog spectrofluorometer before being recirculated through the irradiation cell.

The NAP SOA sample prepared under dry conditions was used in the initial tests of the system. It was irradiated for 46 h with no pH control, and a small change in pH (0.25 SU increase) was observed over the course of irradiation. Therefore, the rest of the experiments were done with active pH control of the irradiated solution. The SOA samples prepared at 40% RH were all irradiated for 44 h at two different controlled pH values. The irradiation time of 44 h under one sun (equivalent to a dose of 6.9 Einstein/m^2 in the 330−380 nm window) is comparable to the typical lifetime of aerosol particles in the atmosphere (a few days). Furthermore, the rate of change in the absorption coefficients became small after 44 h, and further irradiation was deemed unnecessary. A pH of 6 was tested to represent SOA compounds dissolved in cloudwater, whereas a pH of 3 was tested to simulate the more acidic environment of aerosol liquid water or polluted clouds.[36] Even lower pH values have been reported in aerosol particles,[36] but achieving a pH value below 3 would be problematic with this photolysis system. EEMs and absorption spectra were collected for each sample in 20 min intervals using a 0.4 s integration time. Excitation scans and absorption spectra were collected from 230 to 600 nm in 3 nm intervals. Emission spectra were collected from 210 to 618 nm in 3.27 nm intervals. Fluorescence intensities were converted into Quinine Sulfate Units (QSU) after correcting for the Rayleigh and Raman scattering and inner filter effects using previously described methods.[2,37] The absorption data were used to create kinetics plots at 260, 365, 405, and 532 nm. The change in fluorescence apparent quantum yield (AQY) over the course of irradiation was calculated using fluorescence intensities and values given by Brouwer for quinine sulfate in 0.1 M $HClO_4$.[38,39]

DOI: 10.1021/acsearthspacechem.7b00153
ACS Earth Space Chem. 2018, 2, 235−245

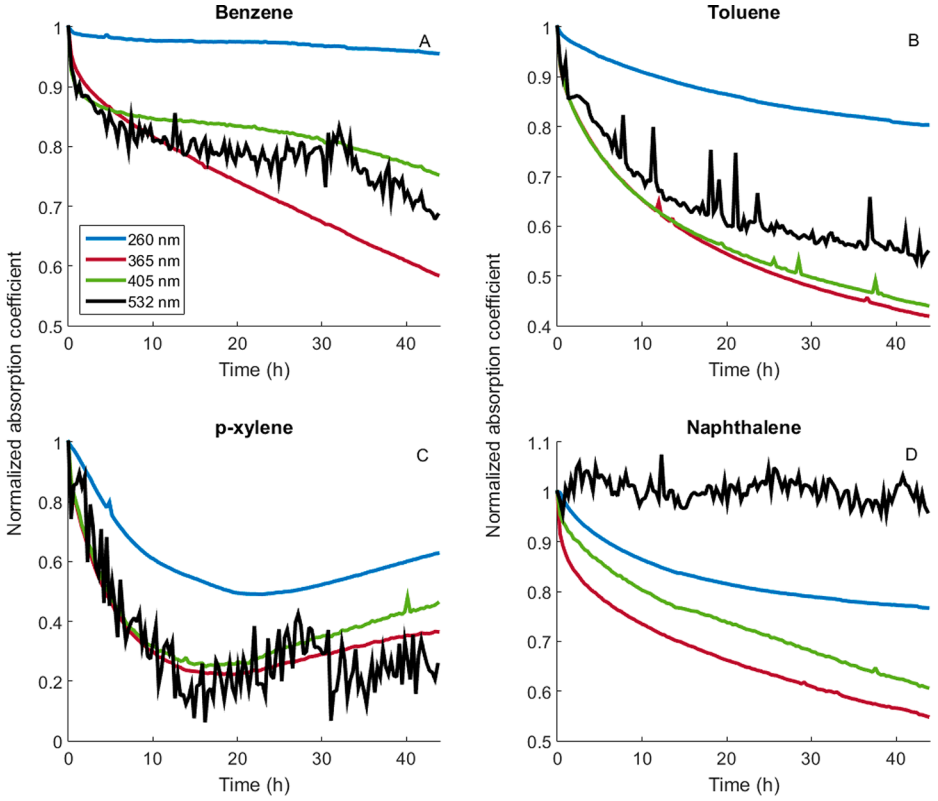

Figure 3. Kinetics plots for samples photolyzed at pH 3 (panels A, BEN SOA; B, TOL SOA; C, XYL SOA; D, NAP SOA) showing the effect of UV radiation on relative absorption coefficients (normalized to zero time) at 260, 365, 405, and 532 nm. The 532 nm trace is noisier than the rest of the traces because the absorption coefficient at this wavelength is small.

2. RESULTS

2.1. Effect of Photolysis on the Absorption Spectra.

Figures 1 and 2 compare absorption coefficients ($\alpha_{solution}$ in m^{-1}) for the solutions of BEN, TOL, XYL, and NAP SOA when irradiated for 44 h at pH 3 and pH 6, respectively. In addition, Figure S1 in the Supporting Information shows the initial values of $\alpha_{solution}$ for all samples before the irradiation. To produce these figures, the measured base-10 absorbance values (A_{10}) were converted into base-e solution absorption coefficients by normalizing to the cell path length (l)

$$\alpha_{solution}(\lambda) = \frac{A_{10}(\lambda) \times \ln(10)}{l} \quad (1)$$

Because of the low mass concentration of SOA in the solution (C_{mass}, given in the last column of Table 1) we can safely assume complete extraction of the SOA material into solution. Therefore, we can get the bulk mass absorption coefficient (MAC_{bulk} in m^2/kg) of the SOA material by normalizing $\alpha_{solution}$ to C_{mass}

$$MAC_{bulk}(\lambda) = \frac{\alpha_{solution}(\lambda)}{C_{mass}} \quad (2)$$

The observed MAC_{bulk} values are comparable to values reported in previous studies. For example, Lee et al. reported MAC_{bulk} = 0.6 m^2/g for NAP SOA at 300 nm,[16] and the corresponding value estimated from the data in Figure S1 is $MAC_{bulk} \sim 1$ m^2/g.

The solution absorption coefficients generally decreased during photolysis. To see the changes more clearly, panels B, D, F, H of Figures 1 and 2 show differences in the absorption coefficient relative to the value before photolysis. Both the initial absorption coefficient and the difference in absorption coefficient depend on pH. Figure S1 provides a comparison of the absorption spectra of each SOA at pH 3 and pH 6 at t = 0 to show that the solution are absorbing stronger at pH 6 across the entire absorption spectrum. Photooxidation of aromatic compounds under high NO_x conditions is known to produce nitrophenols, which make the dominant contribution to the absorption coefficient.[17] The acid–base equilibria of nitrophenols are well-known to cause a strong pH dependence in absorption spectra.[16,40] With a typical pK_a of ~7, the fraction of nitrophenols ionized at pH 3 is very small. However, at pH 6, nitrophenols will be partially ionized and the absorption spectrum will have a contribution from the anions, which have red-shifted absorption spectra compared to the nonionized nitrophenols.[41−45] As a result, the absorption coefficient is enhanced at pH 6 (Figure S1). These are important characteristics because depending on the atmospheric environment where these compounds end up they can have different effects on the absorption of solar radiation. In an acidic environment, which is representative of aerosol liquid water,[36] BrC would absorb less visible sunlight than it would under more neutral conditions in cloud and fog droplets.[46,47]

In all the SOA samples, there was a decrease in the measured absorption coefficients over the irradiation time at all visible wavelengths (Figures 1 and 2). For BEN and TOL SOA, the decrease was the largest at 350 nm, where nitrophenols are known to absorb. In addition to nitrophenols, quinones in NAP SOA can also absorb at visible wavelengths (for example, 1,4-naphthoquinone is yellow). The absorption coefficient around 260 nm was less affected by radiation, and in fact a distinct

DOI: 10.1021/acsearthspacechem.7b00153
ACS Earth Space Chem. 2018, 2, 235−245

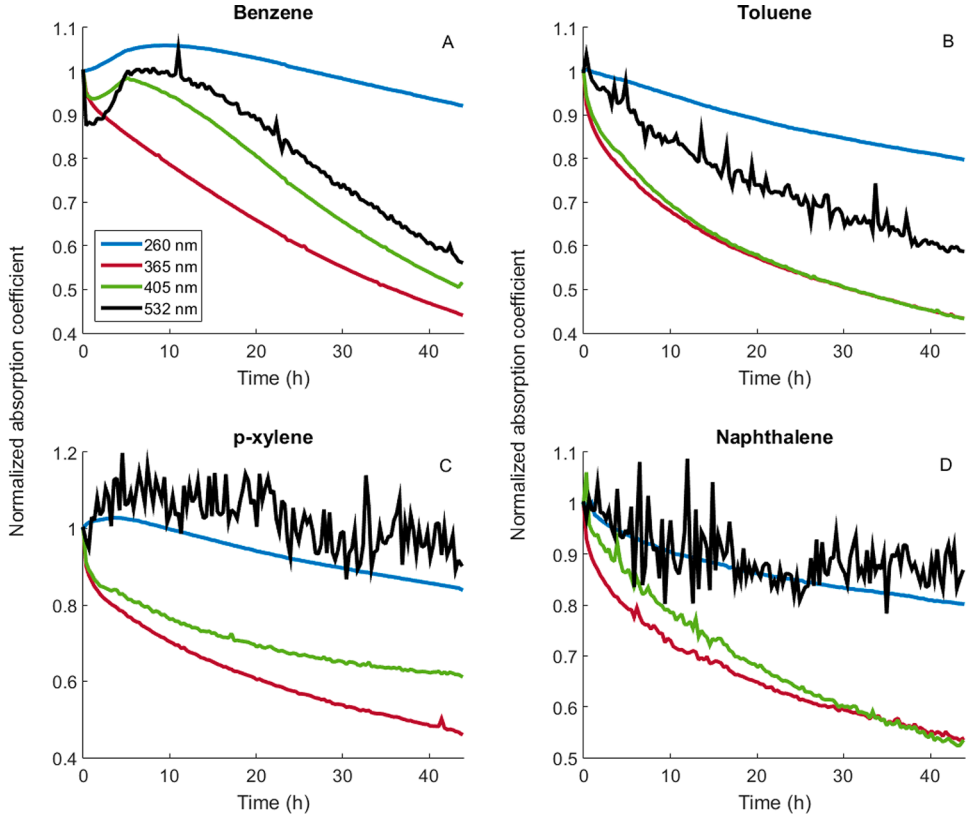

Figure 4. Kinetics plots for samples photolyzed at pH 6 (panels A, BEN SOA; B, TOL SOA; C, XYL SOA; D, NAP SOA) showing the effect of UV radiation on relative absorption coefficients (normalized to zero time) at 260, 365, 405, and 532 nm.

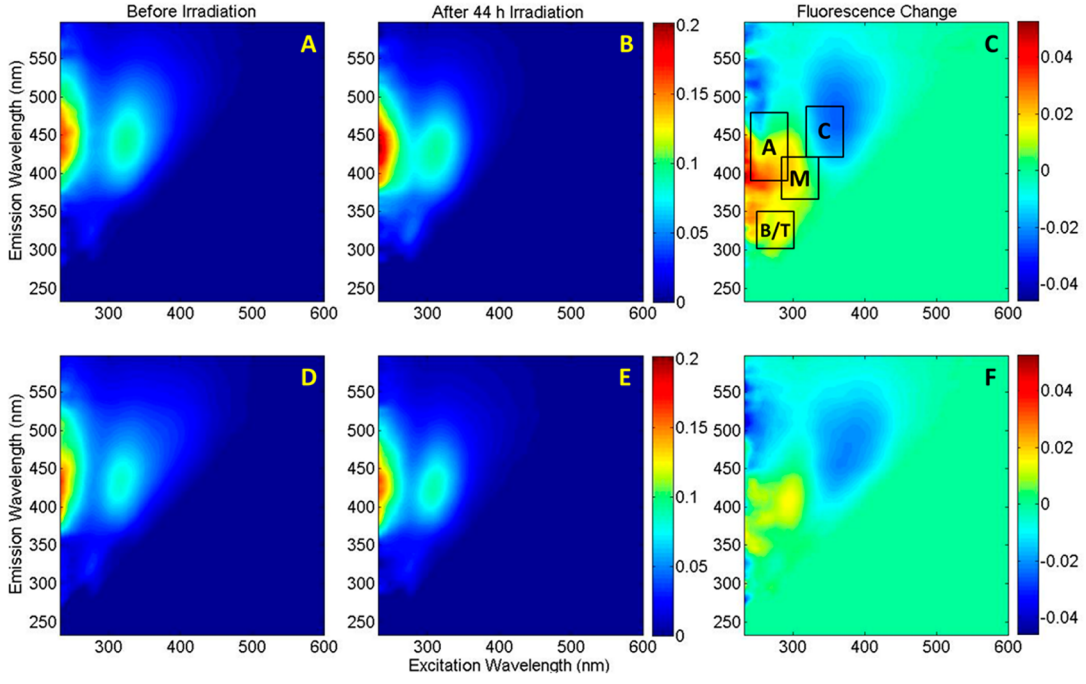

Figure 5. Fluorescence data for BEN SOA sample before (A,D) and after (B,E) 44 h of irradiation at pH 3 (top) and pH 6 (bottom), as well as the overall change in fluorescence (C,F). Common CDOM peaks listed in Table 1 are labeled with boxes in subfigure C.

absorption band grew at this wavelength in some of the samples. This effect was the strongest in BEN SOA at pH 6, which showed an initial increase in absorption coefficient at 260 nm, whereas XYL SOA at pH 3 showed a weaker increase after 20 h of irradiation. Other experiments, such as TOL SOA at pH 3 and pH 6, did not show an increase in absorption coefficient but rather a decreased rate of absorption loss at 260 nm, resulting in the same distinct band. This suggests the presence of photostable compounds in the SOA, which are produced during irradiation in some samples and absorb at 260 nm.

DOI: 10.1021/acsearthspacechem.7b00153
ACS Earth Space Chem. 2018, 2, 235−245

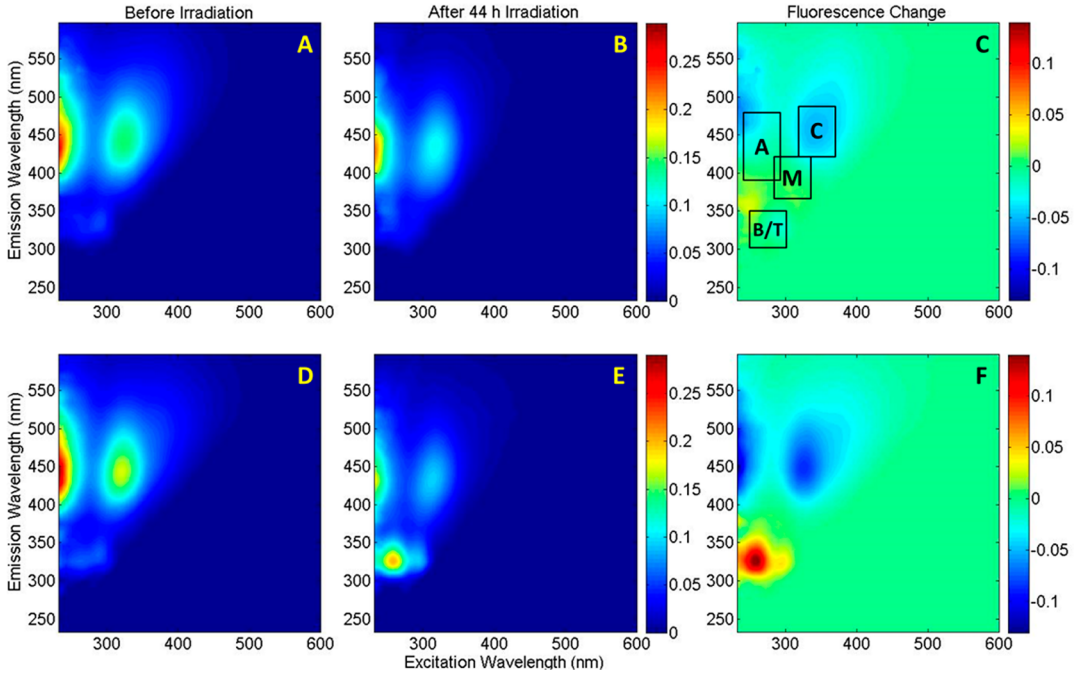

Figure 6. Fluorescence data for TOL SOA sample before (A,D) and after (B,E) 44 h of irradiation at pH 3 (top) and pH 6 (bottom), as well as the overall change in fluorescence (C,F). Common CDOM peaks listed in Table 1 are labeled with boxes in subfigure C.

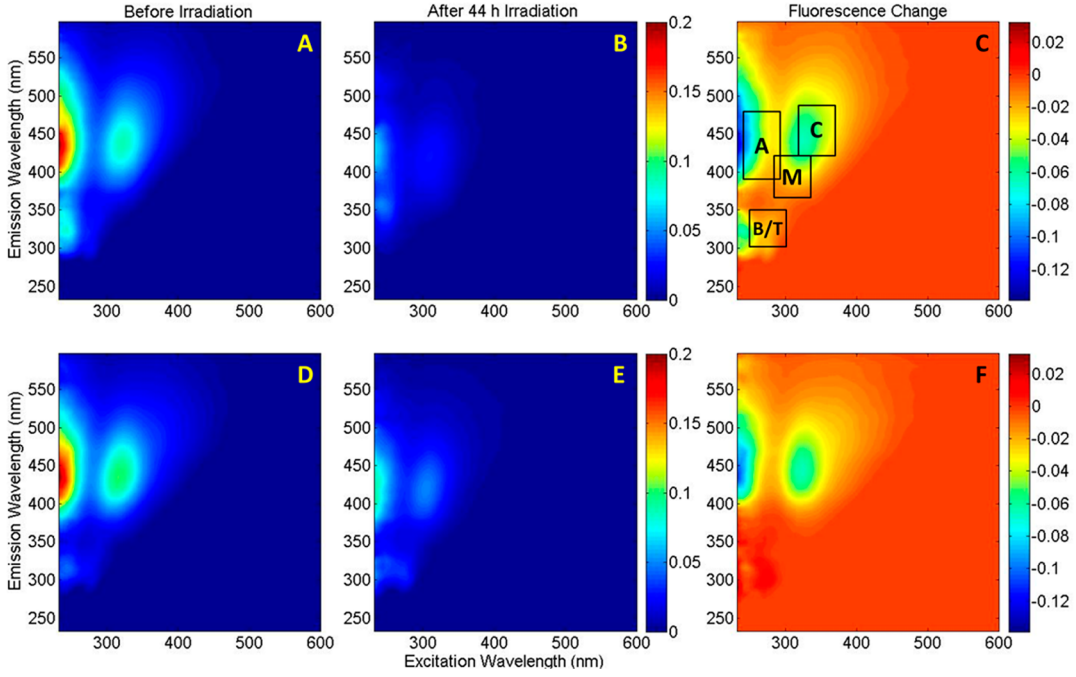

Figure 7. Fluorescence data for XYL SOA sample before (A,D) and after (B,E) 44 h of irradiation at pH 3 (top) and pH 6 (bottom), as well as the overall change in fluorescence (C,F). Common CDOM peaks listed in Table 1 are labeled with boxes in subfigure C.

These observations are consistent with results of aqueous photooxidation of 4-nitrocatechol and related compounds in experiments by Zhao et al.[48] Direct photolysis and aqueous reaction by the hydroxyl radical led to rapid photobleaching of the nitrophenols, as well as a decrease in absorption coefficient at 350 nm and increase at 260 nm.[48]

The rate at which absorption coefficients of BrC change is an important parameter for predicting radiative forcing by BrC. If BrC photobleaches rapidly, it will have less of an overall effect on climate. Figures 3 and 4 show the kinetics plots for each SOA at pH 3 and pH 6, respectively. The chosen wavelengths include 260 (where an absorption band appears during irradiation), 365, 405, and 532 nm (wavelengths at which optical properties of aerosols are commonly measured). The 365 and 405 nm wavelengths represent shorter wavelengths in the solar spectrum, where BrC has been found to contribute 10−30% of total absorption by fine particles, whereas 532 nm falls in the visible region where BrC contributes about 10% of the total absorption.[49] The peak of the solar spectrum also occurs close to 532 nm. The kinetics at 365 and 405 nm follow

DOI: 10.1021/acsearthspacechem.7b00153
ACS Earth Space Chem. 2018, 2, 235−245

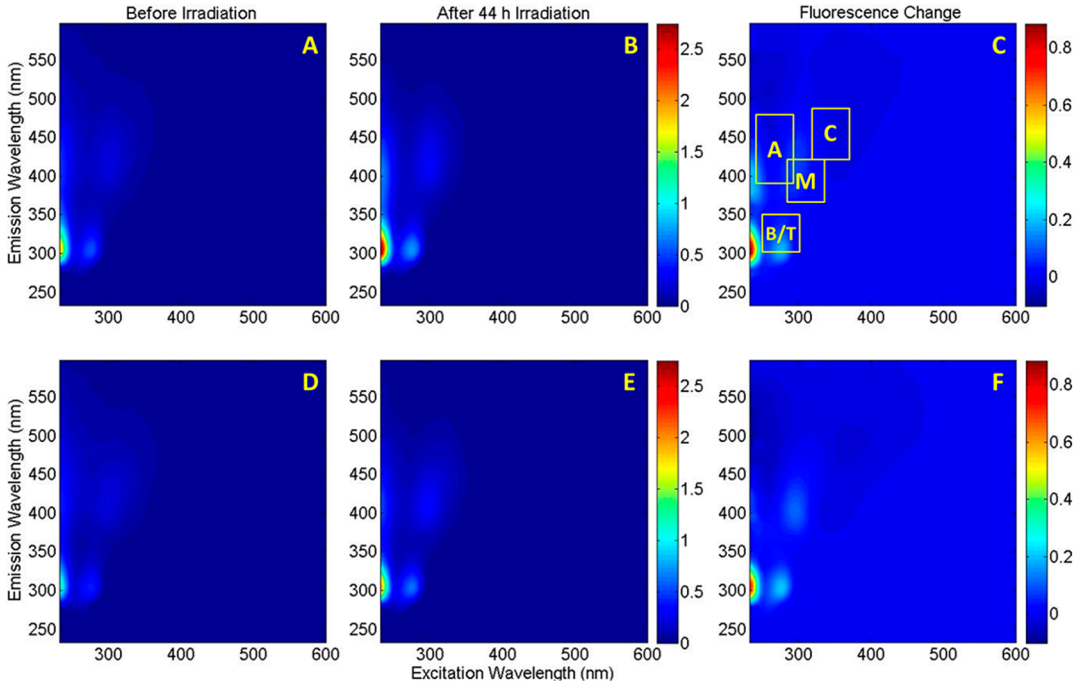

Figure 8. Fluorescence data for NAP SOA sample before (A,D) and after (B,E) 44 h of irradiation at pH 3 (top) and pH 6 (bottom), as well as the overall change in fluorescence (C,F). Common CDOM peaks listed in Table 1 are labeled with boxes in subfigure C.

similar trends in all samples with the absorption coefficients of SOA decreasing by more than a factor of 2 over 44 h (Figure 3 and 4) in a majority of samples. In the TOL and BEN SOA at pH 3 and 6 and XYL at pH 3, the trace at 532 nm also decreases significantly. These observations indicate that as these SOA in the atmosphere are exposed to sunlight, their radiative forcing will diminish.

2.2. Effect of Photolysis on Excitation−Emission Matrix Spectra. Figures 5−8 show the EEM data for all four SOA samples irradiated at both pH 3 and 6 for 44 h. Unlike the reduction in the visible absorption coefficient across all SOA samples, the fluorescence intensity decreased for some excitation−emission wavelength pairs but increased for others. Increases in fluorescence may indicate the formation of new fluorophores or the loss of quenching compounds/moieties, leading to a higher observed quantum yield of fluorescence.[50] There were also small differences between samples irradiated at pH 3 and pH 6, but again the differences were not uniform among the four SOA samples.

BEN SOA displayed two distinct peaks in the EEM spectrum at ex/em = 220/430 and 320/430 at both pH 3 (Figure 5a) and pH 6 (Figure 5d). After the irradiation, there was a broad region around 220−300/400 nm where the fluorescence increased. This region showed no distinct peaks when irradiated at pH 3 (Figure 5c), but irradiation at pH 6 resulted in the increase of a more defined peak centered around 300/400 nm (Figure 5f). Fluorescence decreased at both pH 3 and pH 6 centered at 375/450 nm, similar to component C4 in Timko et al., generally attributed to terrestrial humic-like components of CDOM.[2,4,5] The rate of fluorescence loss increased with pH, similar to previous reports on terrestrial CDOM.[7]

The EEM spectra of TOL SOA shown in Figure 6a for pH 3 and Figure 6d for pH 6 were similar to those of BEN SOA before the irradiation. However, the EEM spectra after irradiation showed greater change at pH 6 than at pH 3. There was a large increase in fluorescence intensity at 250/325 nm at pH 6, but almost no change at pH 3. The fluorescence decreased at 220/450 and at 330/450 nm, and the decrease was stronger in the pH 6 sample. Although the peak at 250/325 nm is often attributed to autochthonous sources when found in CDOM, small aromatic molecules such as *p*-cresol fluoresce in this region.[5,39,51] The longer-wavelength peaks that decreased during irradiation were similar to the decreasing terrestrial humic-like peaks seen in the BEN SOA.

The initial EEM spectra of XYL SOA shown in Figure 7a,d were also similar to the corresponding spectra of BEN SOA and TOL SOA. However, the effect of irradiation on the EEM spectrum of XYL SOA was considerably stronger with fluorescence decreasing by more than a factor of 2 at some fluorescence wavelengths. This is a little easier to see in one-dimensional fluorescence spectra at ex = 250 and 330 nm shown in Figures S2 and S3, respectively. The EEM peak at 220/325 nm had a minimal increase at pH 6, but decreased at pH 3. XYL SOA also has peaks that decrease in intensity centered at 220/450 nm and 330/450 nm at both pH values. These are once again terrestrial humic-like peaks, which fall in the photolabile region.[2,7]

Fluorescence of the NAP SOA samples was quite different from that in BEN, XYL, and TOL samples. The maximum fluorescence intensity was greater for NAP SOA than for the rest of the SOA samples. The spectrum was dominated by a strong peak at 220/300 nm, characteristic of low molecular weight aromatic compounds (Figure 8). This peak increased in intensity by ∼50% during irradiation, with a greater fluorescence increase at pH 3 than pH 6. There were two weaker peaks at 275/300 nm and 310/430 nm both of which showed similar increases of ∼50% in intensity. Lee et al.[16] recorded an EEM spectrum of NAP SOA at a higher solution concentration, and they only reported the 310/430 nm peak, which also increased in intensity after UV irradiation.

DOI: 10.1021/acsearthspacechem.7b00153
ACS Earth Space Chem. 2018, 2, 235−245

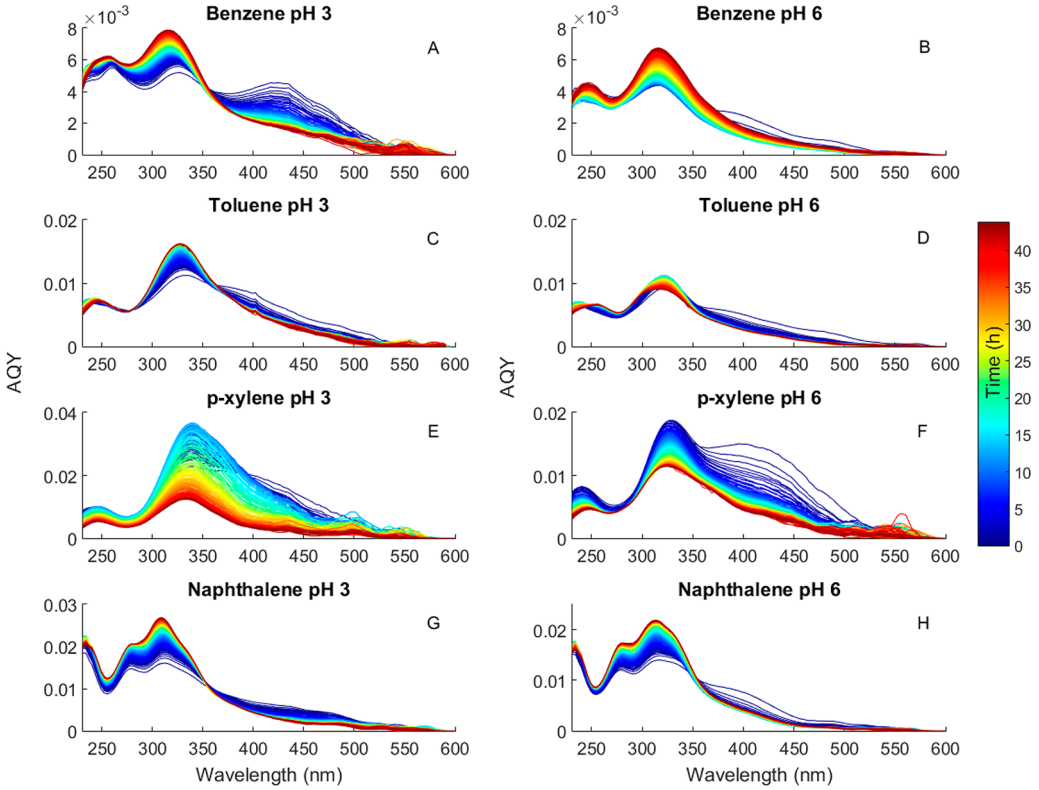

Figure 9. Plots showing the change in apparent quantum yield (AQY) for each SOA sample (BEN SOA, panels A and B; TOL SOA, panels C and D; XYL SOA, panels E and F; and NAP SOA, panels G and H) over the course of 44 h at pH 3 (left) and pH 6 (right).

Although the fluorescence intensity changes are not as consistent as the absorption coefficient change, there is a decrease for all samples in the 325−375 nm excitation and 425−475 nm emission range, which corresponds to the C peak, often attributed to terrestrial humic-like components of CDOM in natural water samples.[4,5] Chen et al. found that water-soluble organic material found in aerosols tend to fluoresce in this region when the species are highly oxygenated with terrestrial and marine origins.[52] Duarte et al. also produced EEMs of water-soluble organic components in aerosols that were similar to those produced for BrC formed by BEN SOA, TOL SOA, and XYL SOA, although the peaks were slightly shifted.[27] This component was found to be photolabile, as seen in the decrease in fluorescence intensity here and in component C4 in Timko et al.[2] Additionally, Yamashita et al. found that there is a strong correlation between lignin derived phenols and this peak.[53] Therefore, nitrophenols responsible for the pH dependence seen in absorption coefficient may also be responsible for the decrease in fluorescence at this peak.

The difference in the location of fluorescence peaks and their response to irradiation shows that, although all of these samples are considered to be types of BrC SOA, each precursor produces compounds with different fluorescent properties. Overall, BrC SOA samples seem to have similar characteristics to CDOM found in fresh water with contributions from terrestrial plant material. Additionally, TOL, XYL, and NAP SOA all showed fluorescence changes in the UVA (320 to 400 nm) portion of the EEM. While peaks in this region are often associated with autochthonous, protein-like material due to the fluorescence of tryptophan and tyrosine, fluorescence changes in these samples are more likely the result of production/destruction of small aromatic molecules.[39]

Information about the fluorescence apparent quantum yield (AQY) for BrC aerosols is important for understanding the effect of BrC on climate. If BrC compounds fluoresce with high efficiency only a fraction of the absorbed radiative energy will be converted into heat, diminishing the heating effect of BrC. At the present time, only a few studies reported AQY for BrC. For example, Lee et al. reported AQY of 0.2% for BrC produced from photooxidation of NAP SOA and 2% for BrC from the methyl glyoxal and ammonium sulfate reaction.[16] Using the fluorescence data in Figures 5−8, the change in AQY over the 44 h irradiation period was calculated and plotted in Figure 9. In all of the SOA samples, both the initial AQY and photoinduced changes are wavelength- and pH-dependent. For example, for TOL SOA at pH = 3, AQY grows with photolysis below 350 nm but is reduced above 350 nm. However, for all of these SOA samples, the AQY values are generally quite small with the peak value of 4% for XYL SOA. This means that fluorescence by this type of BrC is not likely to affect the radiative forcing by aerosols because most of the absorbed solar energy will not be reradiated, but available for heating the atmosphere.

CONCLUSIONS

In this study, we examined how the absorption coefficient and fluorescence spectra of BrC aerosols prepared by high-NO_x photooxidation of common aromatic compounds are affected by solar radiation. The aqueous extracts of SOA prepared from benzene, toluene, *p*-xylene, and naphthalene were found to absorb radiation in the near-UV and visible ranges of the spectrum. The absorption coefficients depended on the solution pH, with the solutions at pH 6 (representative of cloudwater) absorbing stronger than solutions at pH 3

DOI: 10.1021/acsearthspacechem.7b00153
ACS Earth Space Chem. 2018, 2, 235−245

(representative of aerosol and polluted fogwater). The change in the absorption coefficient with pH is due to the acid−base ionization equilibria of phenols, which have very different absorption spectra in ionized and nonionized forms. The absorption coefficients were reduced upon exposure to solar irradiation, especially at visible wavelengths. The photolysis-induced changes in the absorption coefficient and fluorescence spectra mean that the climate effect of these types of BrC SOA will be evolving as the aerosols are aging in the atmosphere. Variations in fluorescence intensity were also observed in several regions of EEM spectra for all four SOA samples. The apparent fluorescence quantum yield was small, of the order of a few percent, which is in agreement to previous fluorescence quantum yield measurements. This indicates that fluorescence is not likely to affect the strength of radiative forcing by this type of BrC. Lastly, the EEM spectra of BrC could be related to EEM spectra of CDOM found in different water systems. The humic characteristics of BrC SOA appeared to be similar to the organic matter found in fresh water with contributions from terrestrial plants. This suggests that deposition of BrC into water systems could contribute to the pool of CDOM in fresh water.

■ ASSOCIATED CONTENT

Supporting Information

The Supporting Information is available free of charge on the ACS Publications website at DOI: 10.1021/acsearthspacechem.7b00153.

Figure S1 (a comparison of solution absorption coefficients before photolysis), Figure S2 (fluorescence spectra at λ_{ex} = 250 nm), and Figure S3 (fluorescence spectra at λ_{ex} = 330 nm) (PDF)

■ AUTHOR INFORMATION

Corresponding Author

*Phone: 949-824-1262. E-mail:nizkorod@uci.edu.

ORCID

Jenna L. Luek: 0000-0002-1343-5375

Sergey A. Nizkorodov: 0000-0003-0891-0052

Notes

The authors declare no competing financial interest.

■ ACKNOWLEDGMENTS

P.A. acknowledges funding by the National Science Foundation Graduate Fellowship Program and the Ford Foundation Predoctoral Fellowship program. This is contribution 5462 of the University of Maryland Center for Environmental Science.

■ REFERENCES

(1) Sharpless, C. M.; Blough, N. V. The importance of charge-transfer interactions in determining chromophoric dissolved organic matter (CDOM) optical and photochemical properties. *Environ. Sci.: Processes Impacts* **2014**, *16*, 654−671.

(2) Timko, S. A.; Maydanov, A.; Pittelli, S. L.; Conte, M. H.; Cooper, W. J.; Koch, B. P.; Schmitt-Kopplin, P.; Gonsior, M. Depth-dependent photodegradation of marine dissolved organic matter. *Front. Mar. Sci.* **2015**, *2* (66), 1−13.

(3) Hudson, N.; Baker, A.; Reynolds, D. Fluorescence analysis of dissolved organic matter in natural, waste and polluted waters-a review. *River Res. Applic.* **2007**, *23* (6), 631−649.

(4) Coble, P. G. Characterization of marine and terrestrial DOM in seawater using excitation-emission matrix spectroscopy. *Mar. Chem.* **1996**, *51* (4), 325−346.

(5) Coble, P. G. Marine optical biogeochemistry: The chemistry of ocean color. *Chem. Rev.* **2007**, *107* (2), 402−418.

(6) Zhao, Z.; Gonsior, M.; Luek, J.; Timko, S. I. H.; Hertkorn, N.; Schmitt-Kopplin, P.; Fang, X.; Zeng, Q.; Jiao, N.; Chen, F.; et al. Picocyanobacteria and deep-ocean fluorescent dissolved organic matter share similar optical properties. *Nat. Commun.* **2017**, *8*, 15284.

(7) Timko, S. A.; Gonsior, M.; Cooper, W. J. Influence of pH on fluorescent dissolved organic matter photo-degradation. *Water Res.* **2015**, *85*, 266−274.

(8) Pinnick, R. G. E.; Fernandez, E.; Rosen, J. M.; Hill, S. C.; Wang, Y.; Pan, Y. L. Fluorescence spectra and elastic scattering characteristics of atmospheric aerosol in Las Cruces, New Mexico, USA: Variability of concentrations and possible constituents and sources of particles in various spectral clusters. *Atmos. Environ.* **2013**, *65*, 195−204.

(9) Matos, J. T.; Freire, S. M.; Duarte, R. M.; Duarte, A. C. Natural organic matter in urban aerosols: Comparison between water and alkaline soluble components using excitation−emission matrix fluorescence spectroscopy and multiway data analysis. *Atmos. Environ.* **2015**, *102*, 1−10.

(10) Hawkins, L. N.; Lemire, A. N.; Galloway, M. M.; Corrigan, A. L.; Turley, J. J.; Espelien, B. M.; De Haan, D. O. Maillard chemistry in clouds and aqueous aerosol as a source of atmospheric humic-like substances. *Environ. Sci. Technol.* **2016**, *50* (14), 7443−7452.

(11) Phillips, S. M.; Smith, G. D. Light absorption by charge transfer complexes in brown carbon aerosols. *Environ. Sci. Technol. Lett.* **2014**, *1* (10), 382−386.

(12) Phillips, S. M.; Smith, G. D. Further evidence for charge transfer complexes in brown carbon aerosols from excitation−emission matrix fluorescence spectroscopy. *J. Phys. Chem. A* **2015**, *119* (19), 4545−4551.

(13) Lee, H. J.; Laskin, A.; Laskin, J.; Nizkorodov, S. A. Excitation-emission spectra and fluorescence quantum yields for fresh and aged biogenic secondary organic aerosols. *Environ. Sci. Technol.* **2013**, *47* (11), 5763−5770.

(14) Pöhlker, C. J.; Huffman, J. A.; Pöschl, U. Autofluorescence of atmospheric bioaerosols − fluorescent biomolecules and potential interferences. *Atmos. Meas. Tech.* **2012**, *5*, 37−71.

(15) Laskin, A.; Laskin, J.; Nizkorodov, S. A. Chemistry of atmospheric brown carbon. *Chem. Rev.* **2015**, *115*, 4335−4382.

(16) Lee, H. J.; Aiona, P. K.; Laskin, A.; Laskin, J.; Nizkorodov, S. A. Effect of solar radiation on the optical properties and molecular composition of laboratory proxies of atmospheric brown carbon. *Environ. Sci. Technol.* **2014**, *48*, 10217−10226.

(17) Liu, J. M.; Lin, P.; Laskin, A.; Laskin, J.; Kathmann, S. M.; Wise, M.; Caylor, R.; Imholt, F.; Selimovic, V.; Shilling, J. E. Optical properties and aging of light-absorbing secondary organic aerosol. *Atmos. Chem. Phys.* **2016**, *16* (19), 12815−12827.

(18) Romonosky, D. E.; Ali, N. N.; Saiduddin, M. N.; Wu, M.; Lee, H. J.; Aiona, P. K.; Nizkorodov, S. A. Effective absorption cross sections and photolysis rates of anthropogenic and biogenic secondary organic aerosols. *Atmos. Environ.* **2016**, *130*, 172−179.

(19) Montoya-Aguilera, J.; Horne, J. R.; Hinks, M. L.; Fleming, L. T.; Perraud, V.; Lin, P.; Laskin, A.; Laskin, J.; Dabdub, D.; Nizkorodov, S. A. Secondary organic aerosol from atmospheric photooxidation of indole. *Atmos. Chem. Phys.* **2017**, *17*, 11605−11621.

(20) Smith, J. D.; Kinney, H.; Anastasio, C. Phenolic carbonyls undergo rapid aqueous photodegradation to form low-volatility, light-absorbing products. *Atmos. Environ.* **2016**, *126*, 36−44.

(21) Chang, J. L.; Thompson, J. E. Characterization of colored products formed during irradiation of aqueous solutions containing H_2O_2 and phenolic compounds. *Atmos. Environ.* **2010**, *44* (4), 541−551.

(22) Gelencser, A.; Hoffer, A.; Kiss, G.; Tombacz, E.; Kurdi, R.; Bencze, L. In-situ formation of light-absorbing organic matter in cloud water. *J. Atmos. Chem.* **2003**, *45* (1), 25−33.

(23) Kampf, C. J.; Filippi, A.; Zuth, C.; Hoffmann, T.; Opatz, T. Secondary brown carbon formation via the dicarbonyl imine pathway: nitrogen heterocycle formation and synergistic effects. *Phys. Chem. Chem. Phys.* **2016**, *18* (27), 18353−18364.

DOI: 10.1021/acsearthspacechem.7b00153
ACS Earth Space Chem. 2018, 2, 235−245

(24) Lin, Y. H.; Budisulistiorini, S. H.; Chu, K.; Siejack, R. A.; Zhang, H.; Riva, M.; Zhang, Z.; Gold, A.; Kautzman, K. E.; Surratt, J. D. Light-absorbing oligomer formation in secondary organic aerosol from reactive uptake of isoprene epoxydiols. *Environ. Sci. Technol.* **2014**, *48* (20), 12012−12021.
(25) De Haan, D. O.; Hawkins, L. N.; Welsh, H. G.; Pednekar, R.; Casar, J. R.; Pennington, E. A.; de Loera, A.; Jimenez, N. G.; Symons, M. A.; Zauscher, M. D.; Pajunoja, A. Brown carbon production in ammonium-or amine-containing aerosol particles by reactive uptake of methylglyoxal and photolytic cloud cycling. *Environ. Sci. Technol.* **2017**, *51* (13), 7458−7466.
(26) Kroll, J. H.; Ng, N. L.; Murphy, S. M.; Varutbangkul, V.; Flagan, R. C.; Seinfeld, J. H. Chamber studies of secondary organic aerosol growth by reactive uptake of simple carbonyl compounds. *J. Geophys. Res.* **2005**, *110*, D23207.
(27) Duarte, R. M.; Pio, C. A.; Duarte, A. C. Synchronous scan and excitation-emission matrix fluorescence spectroscopy of water-soluble organic compounds in atmospheric aerosols. *J. Atmos. Chem.* **2004**, *48* (2), 157−171.
(28) Bones, D. L.; Henricksen, D. K.; Mang, S. A.; Gonsior, M.; Bateman, A. P.; Nguyen, T. B.; Cooper, W. J.; Nizkorodov, S. A. Appearance of strong absorbers and fluorophores in limonene-O_3 secondary organic aerosol due to NH_4^+-mediated chemical again over long time scales. *J. Geophys. Res.* **2010**, *115*, D05203.
(29) Graber, E. R.; Rudich, Y. Atmospheric HULIS: How humic-like are they? A comprehensive and critical review. *Atmos. Chem. Phys.* **2006**, *6*, 729−753.
(30) Limbeck, A.; Kulmala, M.; Puxbaum, H. Secondary organic aerosol formation in the atmosphere via heterogeneous reaction of gaseous isoprene on acidic particles. *Geophys. Res. Lett.* **2003**, *30* (19), 1996.
(31) Mukai, H.; Ambe, Y. Characterization of a humic acid-like brown substance in airborne particulate matter and tentative identification of its origin. *Atmos. Environ.* **1986**, *20*, 813−819.
(32) Zappoli, S.; Andracchio, A.; Fuzzi, S.; Facchini, M. C.; Gelencser, A.; Kiss, G.; Krivacsy, Z.; Molnar, A.; Meszaros, E.; Hansson, H. C.; Rosman, K.; Zebuhr, Y. Inorganic, organic and macromolecular components of fine aerosol in different areas of Europe in relation to their water solubility. *Atmos. Environ.* **1999**, *33* (17), 2733−2743.
(33) Santos, P. S.; Otero, M.; Duarte, R. M.; Duarte, A. C. Spectroscopic characterization of dissolved organic matter isolated from rainwater. *Chemosphere* **2009**, *74* (8), 1053−1061.
(34) Aiona, P. K.; Lee, H. J.; Leslie, R.; Lin, P.; Laskin, A.; Laskin, J.; Nizkorodov, S. A. Photochemistry of products of the aqueous reaction of methylglyoxal with ammonium sulfate. *ACS Earth Space Chem.* **2017**, *1*, 522−532.
(35) Zhong, M.; Jang, M. Dynamic light absorption of biomass-burning organic carbon photochemically aged under natural sunlight. *Atmos. Chem. Phys.* **2014**, *14*, 1517−1525.
(36) Herrmann, H.; Schaefer, T.; Tilgner, A.; Styler, S. A.; Weller, C.; Teich, M.; Otto, T. Tropospheric Aqueous-Phase Chemistry: Kinetics, Mechanisms, and Its Coupling to a Changing Gas Phase. *Chem. Rev.* **2015**, *115*, 4259−4334.
(37) Zepp, R. G.; Sheldon, W. M.; Moran, M. A. Dissolved organic fluorophores in southeastern US coastal waters: correction method for eliminating Rayleigh and Raman scattering peaks in excitation-emission matrices. *Mar. Chem.* **2004**, *89* (1−4), 15−36.
(38) Brouwer, A. M. Standards for photoluminescence quantum yield measurements in solution (IUPAC Technical Report). *Pure Appl. Chem.* **2011**, *83* (12), 2213−2228.
(39) Wünsch, U. J.; Murphy, K. R.; Stedmon, C. A. Fluorescence quantum yields of natural organic matter and organic compounds: Implications for the fluorescence-based interpretation of organic matter composition. *Front. Mar. Sci.* **2015**, *2* (98), 1−15.
(40) Vione, D.; Maurino, V.; Minero, C.; Duncianu, M.; Olariu, R. I.; Arsene, C.; Sarakha, M.; Mailhot, G. Assessing the transformation kinetics of 2- and 4-nitrophenol in the atmospheric aqueous phase.Implications for the distribution of both nitroisomers in the atmosphere. *Atmos. Environ.* **2009**, *43* (14), 2321−2327.
(41) Biggs, A. I. A spectrophotometric determination of the dissociation constants of p-nitrophenol andpapaverine. *Trans. Faraday Soc.* **1954**, *50*, 800−802.
(42) Hayon, E.; Ibata, T.; Lichtin, N. N.; Simic, M. Electron and hydrogen atom attachment to aromaticcarbonyl compounds in aqueous solution. Absorption spectra and dissociation constants of ketylradicals. *J. Phys. Chem.* **1972**, *76* (15), 2072−2078.
(43) Zhu, D.; Hyun, S.; Pignatello, J. J.; Lee, L. S. Evidence for $\pi-\pi$ electron donor−acceptor interactionsbetween π-donor aromatic compounds and π-acceptor sites in soil organic matter through pH effectson sorption. *Environ. Sci. Technol.* **2004**, *38* (16), 4361−4368.
(44) Laws, W. R.; Brand, L. Analysis of two-state excited-state reactions. The fluorescence decay of 2-naphthol. *J. Phys. Chem.* **1979**, *83* (7), 795−802.
(45) van Stam, J.; Lofroth, J. E. The protolysis of singlet excited beta-naphthol: A two-day laboratoryexperiment to introduce photophysics. *J. Chem. Educ.* **1986**, *63* (2), 181−184.
(46) Marinoni, A.; Parazols, M.; Brigante, M.; Deguillaume, L.; Amato, P.; Delort, A. M.; Laj, P.; Mailhot, G. Hydrogen peroxide in natural cloud water: Sources and photoreactivity. *Atmos. Res.* **2011**, *101* (1−2), 256−263.
(47) Brantner, B.; Fierlinger, H.; Puxbaum, H.; Berner, A. Cloudwater chemistry in the subcooled dropletregime at Mount Sonnblick (3106 M A.S.L., Salzburg, Austria). *Water, Air, Soil Pollut.* **1994**, *74* (3−4), 363−84.
(48) Zhao, R. A.; Lee, K. Y.; Huang, L.; Li, X.; Yang, F.; Abbatt, J. P. D. Photochemical processing of aqueous atmospheric brown carbon. *Atmos. Chem. Phys.* **2015**, *15*, 6087−6100.
(49) Yuan, J. F.; Huang, X. F.; Cao, L. M.; Cui, J.; Zhu, Q.; Huang, C. N.; Lan, Z. J.; He, L. Y. Light absorption of brown carbon aerosol in the PRD region of China. *Atmos. Chem. Phys.* **2016**, *16*, 1433−1443.
(50) Wang, Z.; Cao, J.; Meng, F. Interactions between protein-like and humic-like components in dissolved organic matter revealed by fluorescence quenching. *Water Res.* **2015**, *68*, 404−413.
(51) Stedmon, C. A.; Nelson, N. B. The Optical Properties of DOM in the Ocean. In *Biogeochemistry of Marine Dissolved Organic Matter*; Hansell, D. A., Carlson, C. A., Eds.; Academic Press: New York, 2015; pp 481−508.
(52) Chen, Q.; Miyazaki, Y.; Kawamura, K.; Matsumoto, K.; Coburn, S.; Volkamer, R.; Iwamoto, Y.; Kagami, S.; Deng, Y.; Ogawa, S.; Ramasamy, S.; Kato, S.; Ida, A.; Kajii, Y.; Mochida, M. Characterization of chromophoric water-soluble organic matter in urban, forest, and marine aerosols by HR-ToF-AMS analysis and excitation−emission matrix spectroscopy. *Environ. Sci. Technol.* **2016**, *50*, 10351−10360.
(53) Yamashita, Y.; Fichot, C. G.; Shen, Y.; Jaffé, R.; Benner, R. Linkages among fluorescent dissolved organic matter, dissolved amino acids and lignin-derived phenols in a river-influenced ocean margin. *Front. Mar. Sci.* **2015**, *2* (92), 1−14.

DOI: 10.1021/acsearthspacechem.7b00153
ACS Earth Space Chem. 2018, 2, 235−245